Proceedings of the ASME 2010 International Mechanical Engineering Congress & Exposition
IMECE2010
November 12-18, 2010, Vancouver, British Columbia, Canada

IMECE2010/39323

DESIGN OF A MICRO-SCALE MAGNETOSTRICTIVE ASYMMETRIC THIN FILM BIMORPH (μMAB) MICROROBOT

Wuming Jing[†], Xi Chen[‡], Sean Lyttle[†], Zhenbo Fu[†], Yong Shi[‡], David J. Cappelleri[†*]
[†]Multi-Scale Robotics and Automation Laboratory
[‡]Active Nanomaterials & Devices Laboratory
Department of Mechanical Engineering
Stevens Institute of Technology
Hoboken, NJ 07030
Email: {wjing, xchen1, slyttle, zfu, Yong.Shi, David.Cappelleri} @stevens.edu

ABSTRACT

This paper presents the design, analysis, and performance results for a mobile microrobot that was designed for competing in the 2010 NIST Mobile Microrobot Challenge. Inspired by a crab-like microrobot driven by pulsating cardiomyocyte cells, an asymmetrically dimensioned magnetostrictive thin film bimorph microrobot has been designed. Utilizing the magnetostrictive principle, different bending and blocking forces occur under the robot's feet due to the in-plane strain generated in the bimorphs by the application of external magnetic fields in the workspace of the microrobot. The differences in the resulting frictional forces drive the movement of the robot body. To calculate and simulate whether the feet of the robot can generate enough force for locomotion, the design was abstracted and translated into a piezoelectric cantilever FEM model. The results are consistent with the magnetostrictive theoretical equations. Microrobot fabrication and test-bed development based on this analysis is shown along with experimental results validating this approach. Finally, a discussion of the performance results and recommendations for future improvements are provided.
Keywords: microrobot, magnetostrictive, bimorph

INTRODUCTION

Microrobotics has emerged recently as the next wave in intelligent systems [1]. Their small size and mass facilitates new operational modes and high operational speeds. These features will lead to new generation of products which have sound application potential in many fields, like electronics, health care, and manufacturing.

In the micro scale, especially submillimeter range, electrostatic forces and electromagnetic forces are two most common methods of locomotion, although other methods also have been demonstrated, including thermal impact drives [2] and piezoelectric crawlers [3]. For the microrobots of submillimeter range, common used power sources like on-board batteries are not easily utilized, so they have only shown up in the research field recently [2–10]. One of the representative mobile microactuators is the untethered scratch drive actuator developed by Donald [4] et al. Floyd, Pawashe, and Sitti [5] have demonstrated microrobots fabricated from a hard magnetic material. Vollmers [6] et al. developed another electromagnetic actuation approach utilizing a resonant drive mechanism.

This paper's microrobot design (Fig.1) is aimed to a mobile microrobot competition [11] organized by the National Institute of Standards and Technology (NIST). The theme of the competition in the past was a microrobotic soccer competition, while this year the focus is more generally applied to the field of microrobotics. The challenge includes three events: 1) Two millimeters dash: this event requires a microrobot to traverse a distance of two millimeters in as short a time as possible; 2) Micro-assembly: manipulate the robot(s) to insert tiny pegs into microscopic holes; 3) Freestyle competition: this event allows

*Address all correspondence to this author.

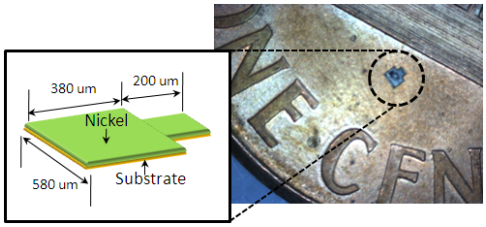

FIGURE 1. μMAB MICROROBOT

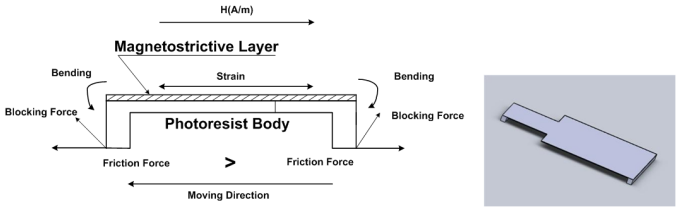

(a) (b)

FIGURE 2. (a) μMAB MICROBOT ACTUATION PRINCIPLE; (b) μMAB SCHEMATIC

teams to highlight the capabilities of their microrobotic technologies by performing a task of their own design. Microrobots used in the events must fit within a 600 μm diameter sphere. The essential requirement is that the robots have to be untethered, without connected wires or attached electrodes for power and control. There are many challenges faced in the design and fabricating microrobot with respect to locomotion, power storage, embedded intelligence and motion measurement, which will accelerate the adoption of the microrobot technology by industry. The team from ETH Zurich has been very successful in past competitions [7] with the wireless resonant magnetic microactuator (WRMMA) *Magmite* family of microrobots. The WRMMA's consists of two nickel masses connected through a gold spring. An attractive magnetic force arises between the initially not magnetized nickel bodies when an external magnetic field is applied. Then, time-variant magnetic fields are used to induce oscillatory motion and it is assumed, impact between the hammer and the body drives the robot forward [6]. The robots from Carnegie Mellon University, utilizing neodymium-iron-boron (NdFeB) [5] magnetic bodies controlled with low frequency magnetic fields have also performed well in previous competitions.

Based on the environment and setting requirement, we choose a magnetic field to provide power for robot locomotion and wireless remote control. In this paper, we will first present the design of the robot, followed by robot modeling and validation. A description of the microrobot fabrication process follows. Next, we describe the experimental system setup and the control strategy. Finally, we conclude with the performance results of the overall system and discuss the problems encountered, recommendations and future work.

MICROROBOT DESIGN

Based on the requirements of the microrobot competition, our objective is to create a remote control microrobot of 600 microns in the largest dimension to perform a series of tasks, which indeed means controlled fast, agile movement. The robot is supposed to be an autonomous agent, not connected by tethers or wires, which means the robot has to harvest power from the exterior environment.

Actuation and Moving Principle

Inspired by Jinsoeok's [12] cell robot design, we apply magnetic fields to provide power and use the magnetostrictive principle to generate motion. In Jinsoeok's cell robot design, cardiomyocytes were cultured on an asymmetric PDMS structure with three front and rear legs. The pulsation of the cardiomyocytes would cause the legs to exhibit vertical bending displacement as a result of the contractile force. The bending causes friction. Finally, the robot motion results from the friction difference between the front legs and the rear legs.

In our design, we apply a magnetostrictive material layer to a substrate layer to generate this contractile force and bending. If the blocking forces of the front leg's bending and rear leg's are different, further, if the following friction difference is larger than the resistance caused by the surface and gravity, motion could be expected. The design and actuation mechanism is shown in the Fig.2.

Thus, we call our robot a **micro**-scale **M**agnetostrictive **A**symmetric thin film **B**imorph (μMAB) microrobot. Magnetostrictive bending, made from a magnetic film bonded to a non-magnetic substrate, occurs when the film is magnetized by an applied field [13]. A magnetostrictive stress is produced in the film. Bending occurs if one end of the two layer structures is clamped. Further, if the deflected end is in contact with some ground or face, a blocking force is produced which is able to provide mechanical work through the friction force it causes. Legs with different geometry dimensions and different contact line/areas are able to lead to different blocking forces and then friction forces. Making use of the friction difference along the contact face between the robot and the arena ground can push or pull the robot mass.

If the external magnetic field is static and constant, the robot legs will remain bent; if the magnetic field is a pulsing signal on and off, the legs will perform bending and straightening, which means a walking/crawling motion will result. Further, when the surrounding magnetic field is with high frequency pulsing signals, for example, with the natural frequency of the robot, the robot would be expected to perform very fast walking and/or running motions. The direction control can be readily realized by changing the direction of magnetic field to align the magnetic

body.

Modeling and Validation Analysis

Determining whether the microrobot has enough power/force to conquer the resistance to move is critical step of validation before manufacturing the μMAB microrobot. We need to calculate how much driving force we can expect based on the common available surroundings, such as off-the-shelf electronics.

To calculate the friction force caused by the blocking force, we need to evaluate the deflection of the magnetostrictive bimorph layers. Except the work in [13], few theories and software tools are able to simulate and predict planar magnetostrictive bimorph's behavior. What we do here is translate the magnetostrictive problems to piezoelectric ones, because the later situation has more available research and analysis software tools such as ANSYS (ANSYS, Inc., *www.ansys.com*) and Coventor (Coventor, Inc., *www.coventor.com*).

Like piezoelectric and its converse effect, piezomagnetic and magnetostrictive effect are opposite phenomena. Neglecting all non-linearities, hysteresis and also the effects of temperature, the piezomagnetic equations are [14]:

$$\varepsilon = \frac{\sigma}{E_y^H} + d_{33}^{\sigma} H \tag{1}$$

$$B = d_{33}^{H^*} \sigma + \mu^{\sigma} H \tag{2}$$

where ε is strain, E_y^H is Young's modulus at constant magnetic field H, B is magnetic induction, μ^{σ} is permeability at constant stress, d_{33}^{σ} is its the axial strain coefficient while d_{33}^{σ}= dε/dH, and $d_{33}^{H^*}$ is its inverse coefficient while $d_{33}^{H^*}$=dB/dσ. Now, we can look at the equations with the ones describing piezoelectric phenomena. The so-called coupled equations for piezoelectric of the strain-charge form are [15, 16]:

$$S = [s^E]T + [d^t]E \tag{3}$$

$$D = [d]T + [\varepsilon^T]E \tag{4}$$

Where S is strain, s is compliance stiffness and T is stress. D is the electric charge density displacement (electric displacement), ε is permittivity and E is zero or constant electric field strength. d is the matrix for direct piezoelectric effect and d^t is the matrix for the converse piezoelectric effect. The superscript E indicates a zero or constant electric field; the superscript T indicates a zero, or constant, stress field; and the superscript t stands for transposition of a matrix.

TABLE 1. Analogies in Piezomagnetic and Piezoelectric Domains

	Magnetostrictive-piezomagnetic	Converse-piezoelectric
Concept	magnetic field	electric field
Symbol&Unit	H(A/m)	E(V/m)
Concept	magnetic induction	electric displacement
Symbol&Unit	B(N/A·m)	D(C/m^2)
Concept	piezomagnetic-strain coefficient	piezoelectric-strain coefficient
Symbol&Unit	d(Vs/N=m/A)	d(C/N=m/V)

Comparing both of the equation sets we can notice that if we treat the effect as a one-dimensional property, the mathematic principles of piezoelectric and piezomagnetic are basically the same. Magnetic field corresponds to the electric field and the other relevant physical quantities corresponding, respectively. All of these analogies are summarized in Table 1. Therefore, for a simple structure, the magnetostrictive phenomenon could be calculated and simulated by the inverse piezoelectric phenomenon and method. For the robot structure shown in Fig.2, we calculate the bending displacement and blocking force through the same dimension, using a silicon substrate cantilever deposited with piezoelectric layer, whose property parameters are modified appropriately. An analytical model for a PZT biomorph cantilever deflection is described in [17]:

$$\delta = \frac{3L^2}{2t} \frac{2AB(1+B)^2}{A^2B^4 + 2A(2B+3B^2+2B^3)+1} dV \tag{5}$$

Where δ is the displacement of the beam structure, L is the beam length, t is the beam thickness (silicon+PZT), A is the Young's modulus ratio of silicon and PZT, B is the thickness ratio of silicon and PZT, d is the piezoelectric coefficient, and V is the electric field in V/m.

As long as we have these theoretical models in the piezoelectric domain, the next step is to evaluate the parameter values in the magnetostrictive domain reasonably. The geometric dimensions are the same values and the values of substrate material properties are also the same in both domains, like Young's modulus. For the magnetostrictive material, we select terfenol-D. Its physical property and magnetostrictive coefficient are evaluated according to the data sheet [18] and relevant literature [19], where we have the Young's modulus of terfenol-D is 30 GPa. The magnetostrictive coefficient d_{33} is 1.5E-8 Vs/N (or m/A), which corresponds to the piezoelectric-strain coefficient. The only undetermined value left is V, which corresponds to the surrounding magnetic/electric field potential difference. Based on the Ampere's circuital law [20], we see that the magnetic field

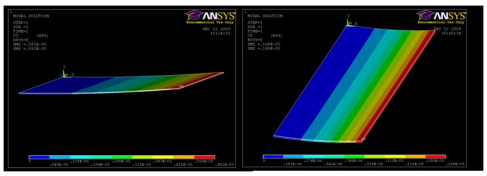

FIGURE 3. DEFLECTION SIMULATION IN ANSYS

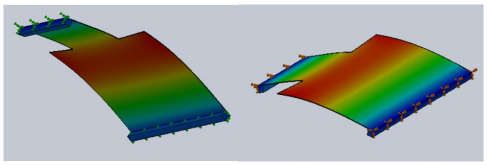

FIGURE 4. NATURAL FREQUENCY SIMULATION IN ANSYS

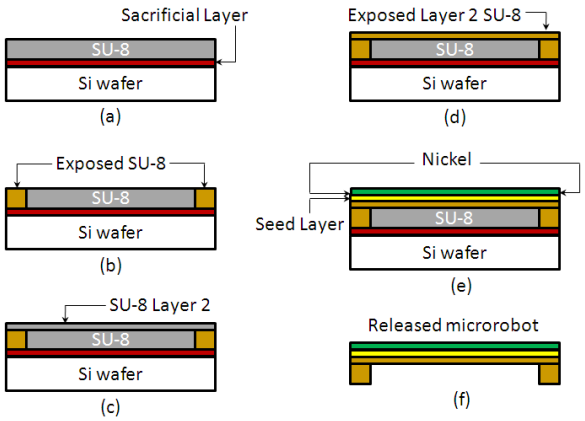

FIGURE 5. Fabrication Process Flow

with as strong as intensity of H = 2000 A/m is able to be expected. Based on these values and Eqn.5, we get a theoretical deflection of about 5.61μm and 1.61μm for the front and rear legs, respectively. These results were also validated through ANSYS, using the piezo units 226 element type, whose results are 5.81μm and 1.68μm (Fig.3). Therefore, the theoretical model is able to predict the real deflection well. Moreover, to calculate the blocking force, we can apply the model in [17] using Eqn.6:

$$F = \frac{3wt^2}{8L}\frac{2AB}{(AB+1)(1+B)}YdV \qquad (6)$$

where F is the maximum blocking force, and w the width of the beam. The maximum theoretical blocking force was calculated based on the coefficient d and material's Young's modulus. The calculation of the difference blocking force from the assymetric design is approximately 5μN. We can compare this driving force with resistive force. For a conservative estimation, we let the friction coefficient = 1 and calculate the drag force to be on the order of nN's. The gravity force is calculated to be approximately 9 nN. Thus, we are able to predict that the drive force is much larger than required (μN vs nN).

Besides the robot deflection and drive force, the lowest natural frequency and the first mode of the robot are also predicted through FEM modeling. This is illustrated in Fig.4, which provides a reference for the primary excitation (control) signal for the microrobot. Fixing the front and rear feet to simulate contact with the ground surface, the simulation result shows that the first natural frequency is at about 6 kHz.

MICROROBOT FABRICATION

This μMAB design was fabricated with custom MEMS technics such as photolithography and electroplating. Fig.5 shows the process flow. The first step (a) is the deposition of positive photoresist on bare silicon wafer as sacrificial layer, followed by coating with one layer of negative photoresist(SU8-100, MicroChem, Inc., *www.microchem.com*). The sacrificial layer is exposed without a mask for the final releasing the robots off the substrate. In step (b) the leg structures are patterned but without development. Next, another thin layer of negative photoresist of type SU8-2 (MicroChem, Inc.) is applied. This layer of SU8-2 is only 2μm thick, which is the thickness we set in the design and simulation for the body of the μMAB. In step (d), the SU8-2 layer is exposed to define the asymmetric body outline. The exposing time of this step is critical, especially over-exposure, because a thicker body would make the robot much harder (stiffer) to bend. Also before resist development, a seed layer of Cu was evaporated for the following electroplating step. The shape of the robot's body is visible after the photolithography post-bake step, which is also evident after the copper evaporation. As these are our initial fabrication trials, nickel not Terfenol-D was chosen as our magnetostrictive layer due to its ease of fabrication, cost and availability. Moreover, our simulation showed the design is able to generate much more power than required, so apply nickel rather than Terfenol-D will be sufficient to actuate the robot, although it's magnetostrictive strain coefficient is lower. After electroplating nickel in a yellow-room environment and cleaning, we use SU8 developer to release the robot from the base structure, as shown in step (f). The sacrificial layer is also released by the SU8 developer. Finally, the robots are extracted after IPA cleaning. Due to stresses in nickel layer and thin substrate, the finished μMAB's exhibit a slightly out-of-plane arched shape at the end of the fabrication process.

Macro-scale robots can be handled easily because they are visible to the naked eye. That's not necessarily the case at the micro-scale. It's not easy and usually hard to pick, handle and move the μMAB's to the testing area. In our case, we can grab them by a small magnet, taking advantage of its magnetic property. The robot's quality can also be judged according to its dif-

ficulty of picking, i.e. easier to pick up robots indicates a thicker magnetic nickel layer. A glass spacer (microscopy slide) was also used between the microrobot and magnet for easier releasing of the robot to the testing area.

EXPERIMENTAL TESTING

Test-bed Design

To participate in the NIST Mobile Microrobotics Challenge at the 2010 IEEE International Conference on Robotics and Automation (ICRA) held in Anchorage, Alaska, a portable microrobotics test-bed was required to be designed and built to enable repeatable live demonstrations. Therefore, the system components were designed for easy assembly and disassembly and to fit the competition size constraints. To move and control the robot as designed, the test-bed setup was designed as shown in Fig. 6. It includes two orthogonal coil pairs to provide a magnetic field. The coil pairs surround a testing platform where the robot moves, and are supported by a machined aluminum column. Computer-controlled drive electronics modulate the coils' operating current and voltage signals.

The robots are actuated and controlled with the magnetic field generated by the coils shown in Fig.6(a) and (c). The small and large coil pairs are made from copper magnetic wire with 110 and 180 turns, with diameters of 2.2" and 3.1", respectively. Solid iron cores can be inserted into each coil to provide increased magnetic field strength in the workspace of the robot. The cores and associated mounting brackets are modular and are not pictured in the figure. The coil pairs are supported by laser-cut acrylic braces along with the testing platform, creating a coil assembly unit. The coil assembly unit sits on two press-fit guide shafts and a threaded rod. The machined aluminum support column has a tapped hole for the threaded rod and two bored out holes for the guide shafts and sleeve bearings to which the coil assembly can mate. A thumb-screw on the threaded rod allows for vertical adjustment of the coil assembly unit relative to the fixed support column. The support column is mounted to a square mounting plate. The robot's performance is observed through an overhead firewire CCD camera (Flea2, Point Grey Research, Inc., *www.ptgrey.com*), a 0.7X to 3X focus lens (VZM 300i, Edmund Optics, *www.edmundoptics.com*), fiber optic light source and light ring (MI-150, Edmund Optics). The camera and lens are mounted on a rack and pinion focusing mount (NT54-793, Edmund Optics) that is attached to a vertical shaft on a circular baseplate. The camera is connected to a control computer to capture real-time images of the robot.

The drive electronics box is hooked up to a two channel 35V/10A variable power supply. A schematic for the circuit connected to channel 1 on the supply is shown in Fig. 7. A similar circuit is connected to the channel 2 on the power supply. Since the magnetic field is determined by the amount of current flowing through the coils, the drive electronics were designed to

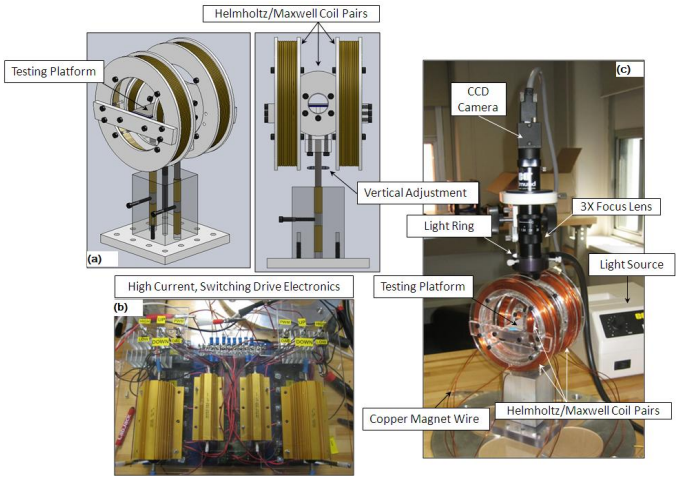

FIGURE 6. PORTABLE MICROROBOTICS TEST-BED

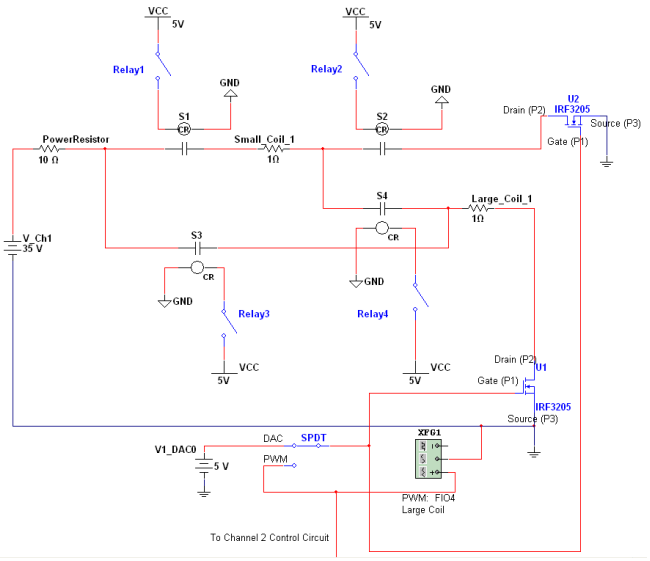

FIGURE 7. CONTROL CIRCUIT FOR CHANNEL 1

adjust the level of current through each coil independently. A series of solid state relays were used to control which of the four coils are activated. Power resistors and supply voltages are set to determine appropriate coil current levels. Two sets of power resistors (5 and 10 Ohm resistances) are used, allowing for high and low power mode operations for each of the coils. The modes are selected with a switch on the drive electronics control box. Also through a switch on the box, the two orthogonal coil pairs can be set to operate in either Helmholz or Maxwell coil pair configurations, allowing for the same or opposite current directions through the coils in the pair, respectively. As shown in the figure, four relays are used to control one small coil and one big coil (i.e. one of the two coils in the coil pair). The relays

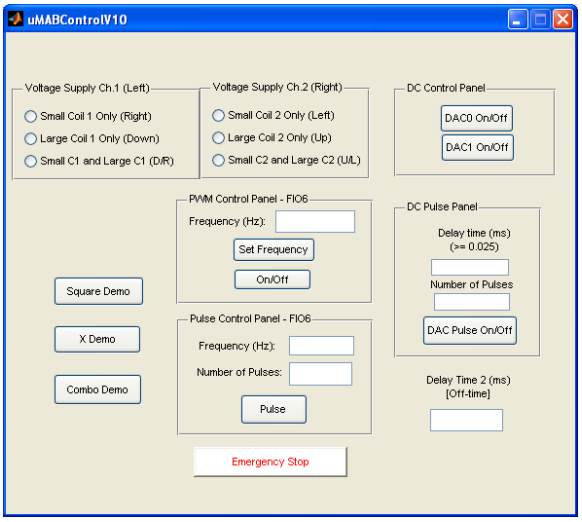

FIGURE 8. μMAB CONTROL GUI

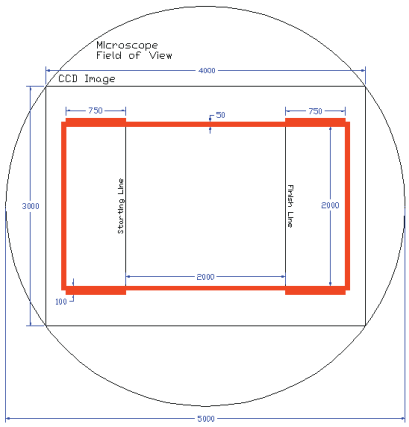

FIGURE 9. ARENA DIMENSIONS (MICRONS) FOR THE TWO MILLIMETER DASH

(coils) can be opened and closed individually or simultaneously. Two high speed, high power MOSFETs (IRF3205, International Rectifier, *www.irf.com*) are used as transistor switches, switching the current flow on/off through the appropriate load (coil) when a sufficient signal on the gate pin is achieved. The control signal to the MOSFETs is either a constant or pulsed signal waveform, providing constant or oscillating external fields to the robot workspace. These control signals, along with the control signals to operate the solid state relays, are sent via computer control of a data acquisition board (LabJack U3-HV and CB15 Board, *www.labjack.com*) with 16 flexible I/O pins. The system is able to pulse signals with a frequencies as high as 40 kHz, which will cover the range of the first few natural frequencies of the μMABs. The electronics can provide up to 6A of current per coil. With an input current of 2A in one coil pair, a magnetic field of about 0.5mT is able to be produced at the center area of the coil pairs, which is enough to drive the robot on a dry, flat substrate. A Matlab©-based graphical user interface was created to operate the system. A screen-shot of the GUI is pictured in Fig.8.

Testing and Results

The required arena dimensions for the Two Millimeter Dash event are shown in Fig.9. Playing fields were constructed by patterning SU-8 photoresist to to the dimensions in shown with the red lines in the figure. The structures, with a height of approximately *50?* μm, were released from the substrate after photoresist development so that they can be placed on top of various substrates for microrobot testing. Microrobot testing was performed on substrates of glass, silicon wafers (both polished and unpolished surfaces), and a combination of sputtered zirconia with a very thin ($\approx$250Å) over-layer of sputtered silica. Testing was conducted with the substrates open to atmospheric conditions as well as some tests with a plastic enclosure surrounding the test-bed and a low flow of nitrogen gas from above to help produce a clean, dry environment for the robots. A number of robots were selected from a couple of fabrication cycles for testing. Most of them are able to move in the magnetic field generated by one single coil. However, the initial tests utilizing glass substrates in an open testing environment provided inconsistent results. The same set of control signals resulted in varied robot performance, ranging from no movement to the robot being driven right off the test-bed at very high speeds. It was determined that the friction forces encountered between the robots legs and the glass substrate was too large and inconsistent to allow for controlled movements. Subsequent tests utilizing the silicon wafer substrates (both polished and unpolished surfaces) and the zirconia/silica substrates, with and without nitrogen, provided more consistent and repeatable results.

The expected actuation modes for the μMABs are shown schematically in Fig.10 and both were verified experimentally. The first actuation mode is due to induced vibration of the robot from an oscillating (pulsing) magnetic field (Fig.10(a)). A pulsed frequency of approximately 4 kHz was applied to the small coil pair, in the Helmholz configuration and the high power mode ($\approx$ 5A/coil), in 20 pulse increments. The pulse signal caused the main body of the robot to vibrate/deflect and the robot to translate across the substrate. At the conclusion of the pulse train, the robot motion ceased. Upon the application of another magnetic field pulse train, robot movement resumed in a similar manner. Snap-shots from one such test illustrating this actuation mode are shown in Fig.11. In this working mode, the robot moves relatively steady and controllable because the end point of each "walking" step is predictable. Although the translation direction is not accordant with the robot's front and rear leg as expected, it shows exact accordance with the magnetic field's direction. It

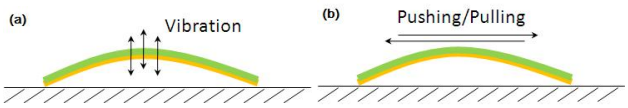

(a) Vibration Actuation from Oscillating Field (b) Pushing/Pulling with Gradient Fields

FIGURE 10. μMAB ACTUATION MODES

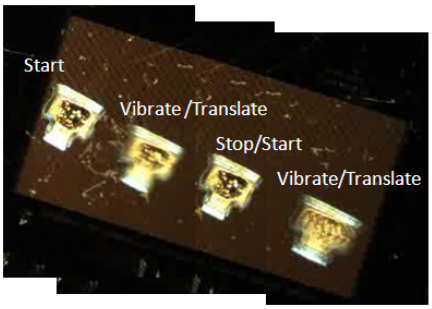

FIGURE 11. PULSED FIELD ACTUATION: μMAB VIBRATION AND TRANSLATION

also shows that the deflection power (force) is much bigger than the frictional resistance generated by gravity, because even a friction difference, not due to the asymmetric structure, is able to translate the robot.

While not all of the robots exhibited the first actuation mode, all robots with an adequate Nickel layer exhibited the second actuation mode consisting of simply pushing or pulling the magnetic body with a magnetic field (Fig.10(b)). In this mode, the magnetized nature of the robot is responsible for the motion. Different currents are input into each coil in a coil pair (small or large) to create a gradient magnetic to direct the magnetic force to translate the μMAB with very fast speeds. This mode was used very successfully in the Two Millimeter Dash event at the challenge. The μMAB achieved one of the fastest individual runs of the competition for the dash at only 27 ms. The average time for the winning team in the Two Millimeter Dash event was 31.67 ms, while the average time for our successful runs was 33.33 ms. Moreover, the translation direction for the μMAB is along with the magnetic field line, which means the translation direction is predictable and controllable. Thus, by creating gradient fields with adjacent coils in the orthogonal sets in different pairs (i.e. one small coil and one large coil) diagonal translation is possible. We took advantage of this controllability in the Freestyle event in the competition, realizing automated horizontal, vertical and diagonal translation through a simple series of commands. Screen-shots illustrating the uMAB's performance under this gradient field actuation is shown in Fig.12.

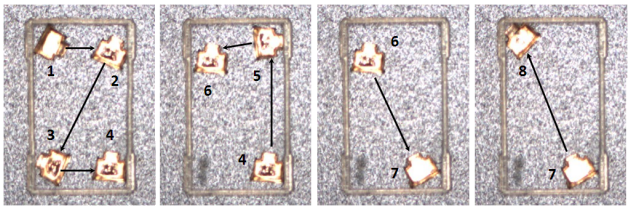

FIGURE 12. GRADIENT FIELD ACTUATION: μMAB XY AND DIAGONAL TRANSLATION

DISCUSSION AND RECOMMENDATIONS

The obtained μMAB performance revealed some important points for the future improvements. The main problem is having the μMAB's exhibit the necessary deflections to allow the vibration mode actuation of the robot to occur. Only a small ratio out of all the robots tested were able to move using the vibration mode as designed, while all robots with a sufficient nickel layer translated in response to the application of gradient magnetic fields. Reasons for this type of performance and resulting recommendations for future work will be explained now.

Modeling

An exact model or tool to analyze the magnetostrictive phenomenon happening in the planar bimorph situation currently does not exist. More importantly, in the magnetic domain, all the material with magnetic properties is initially magnetized. Hysteresis of the magnetic properties is also present. Therefore, it is extremely hard to determine how the magnetized body and magnetostrictive principle of the body are coupled and interact at the micro-scale. Therefore, more accurate theoretical modeling of the planar magnetostrictive bimorph, considering the initial magnetization is necessary for a better prediction of the robot's real performance.

Manufacturing

Another reason for the μMAB's performance and an area for improvement comes from the fabrication process. Based on the design principle, the robot's actuating motion occurs with the vertical deflection of robot's body relative to the substrate. However, it is much harder to control the dimensional accuracy of the robot body's vertical dimension than the planar body dimensions using the current fabrication process. A thicker out-of-plane dimension results in a much stiffer robot. Due to this thickness uncertainty, the actual natural frequency of the robot can vary a lot from the analysis, which makes the determination of the input pulsing signal's frequency much more difficult. Improved or new strategies, either in the microrobot design or manufacturing process, are called for in order to obtain more accurate results for microrobots that utilize the vibration mode actuation scheme.

Environmental Conditions

The dependance on the environmental conditions where the robots move around also need to be stressed has having a major impact on our testing results. The main factors that dominates the robots' performance are the condition and type of the substrate that the robot operates on. The initial tests started with cleaned glass slides and cleaned silicon wafer substrates. The robots worked reasonably well on them at the beginning but the substrates got dirtier as time went by because the sytem was being operated in an open environment in a standard (non-clean) room. Debris, scratches on the slides and wafers, and ambient humidity in the room, made the robots' motion more random than predictable during testing. Next, we turned to the work surface provided by NIST that was used in previous competitions. This is the sputtered zirconia surface with a thin over-layer of sputtered silica. The robots performed much better on this surface because of less drag and stiction. However they got dirty after period of time and scratched and performance decreased. The surfaces were cleaned with compressed air and worked better but did now show as good a result as before. A low flow of nitrogen was used in conjunction with this surface to ensure a dry surface for improved performance. This helped but some problems still remained. The last surface used for testing was the back (unpolished) side of a silicon wafer (with and without a low flow of nitrogen), which turned out to yield the the best results. An explanation for this is the fact that the surface is flat while it also has a gritty quality which can absorb some dirt particles in the air and is harder to scratch than the other surfaces. Therefore, to summarize the lessons learned by testing the robots on various surfaces: (1) Surface condition (roughness, scratches) is a key factor of the robot's performance; (2) Flat and frictional (non-smooth) surfaces are the best for this robot design; and (3) Environmental consistency is necessary to guarantee consistent robot performance. Thus, future work on fabricating a closed system with a sealed space for the robot's arena, conveniently designed for placing in and taking out the robots, will be pursued. Back-side silicon wafer substrates or similar will be used in the chamber.

CONCLUSIONS

A new wireless microrobot design, utilizing an assymetric magnetostrictive bimorph structure was presented here. The magnetic field was generated by two pairs of magnetic coils which are controlled with a high current drive electronics package and a PC. The obtained results reveal that the magnetic and magnetostrictive principle is a promising actuation method for the wireless and remote microrobot. A low magnetic field intensity and gradient have enough energy to power the microrobot. A more complicated microrobot design should be feasible by suitable application of structures using magnetostrictive mechanisms. The results also indicated that more realistic theoretical and FEM calculations are essential to capture the coupling effect of the magnetization and magnetostrictive phenomenon and accurately predict the microrobot performance. Finally, the choice and condition of the substrate for the microrobot to operate on was shown to greatly affect it's performance.

ACKNOWLEDGMENT

The authors would like to acknowledge Prof. Jan Nazalewicz, Mr. Yosef Korogodsky, and Mr. Rino DeFlorio for their help and discussions on the drive electronics. We also acknowledge the Micro-Devices Laboratory at Stevens Institute of Technology, Prof. E.H. Yang, Dr. Daizong Li, and Mr. Anderson Tsai, for providing the fabrication facility and required equipment training needed for this project. The authors would also like to acknowledge Dr. Craig McCray and Dr. Jason Gorman at NIST for organizing the NIST Mobile Microrobotics Challenge and for their discussions on the competition.

REFERENCES

[1] Gorman, J. J., McGray, C. D., and Allen, R. A., 2009. "Mobile microrobot characterization through performance-based competitions". Performance Metrics for Intelligent Systems (PerMIS) Workshop.

[2] Sul, O. J., Falvo, M. R., Taylor, R. M. I., Washburn, S., and Superfine, R., 2006. "Thermally actuated untethered impact-driven locomotive microdevices". Applied Physics Letters, **89**(203512).

[3] Oldham, K., Choong-Ho, R., Jeong-Hoon, R., Polcawich, R., and Pulskamp, J., 2009. "Lateral thin-film piezoelectric actuators for bio-inspired micro-robotic locomotion". Proceedings of the ASME IDETC, San Diego, CA, DETC2009.

[4] Donald, B. R., Levey, C., McGray, C. D., Paprotny, I., and Rus, D., 2006. "An untethered, electrostatic, globally controllable mems microrobot". Journal of Microelectromechanical Systems, **15**(1), February, pp. 1–15.

[5] Floyd, S., Pawashe, C., and Sitti, M., 2008. "An untethered magnetically actuated micro-robot capable of motion on arbitrary surfaces". Proceedings of the IEEE International Conference on Robotics and Automation, Pasadena, CA.

[6] Vollmers, K., Frutiger, D. R., Kratochvil, B. E., and Nelson, B. J., 2008. "Wireless resonant magnetic microactuator for untethered mobile microrobots". Applied Physics Letters, **92**(144103).

[7] Frutiger, D. R., Vollmers, K., Kratochvil, B. E., and Nelson, B. J., 2008. "Small, fast, and under control: wireless resonant magnetic micro-agents". in Proc. Int'l, Symposium on Experimental Robotics.

[8] Pawashe, C., Floyd, S., and Sitti, M., 2009. "Modeling

and experimental characerization of an untethered magnetic micro-robot". Int. J. Robotics Research.

[9] Zhang, L., Abbott, J. J., Dong, L. X., Kratochvil, B. E., Bell, D. J., and Nelson, B. J., 2009. "Artificial bacterial falgella: Fabrication and magnetic control". Applied Physics Letters, **94**(6).

[10] Ghosh, A., and Fischer, P., 2009. "Controlled propulsion of artificial magnetic nanostructured propellers". Nano Letters, **9**(6), pp. 2243–2245.

[11] NIST. "http://www.nist.gov/eeel/semiconductor/mmc/". NIST Mobile Microrobotics Challenge website.

[12] Kim, J., Park, J., Yang, S., and et. al., 2007. "Establishment of a fabrication method for a long-term actuated hybrid cell robot". Lab on a chip.

[13] Marcus, P., 1997. "Magnetostrictive bending of a cantilevered film-substrate system. magnetism and magnetic materials". Magnetism and Magnetic Materials, **168**.

[14] Sasso, C., Pasquale, M., Giudici, L., and et. al., 2006. "Piezomagnetic coefficients of polymer bonded coferrites". Sensors and Actuators A, **129**.

[15] IEEE, 1978. "Ieee std 1976-1978 ieee standard on piezoelectricity". The Institute of Electrical and Electronics Engineers.

[16] Jaffe, B., Cook, R., and Jaffe, H., 1971. Piezoelectric Ceramics. Academic Press, New York, NY.

[17] Fabrice, F. C., Wilson, S. A., Ensell, G., and et. al., 2007. "Characterization of pzt thin film micro-actuators using a silicon micro-force sensor". Sensors and Actuators A, **133**.

[18] Etrema Products. "http://www.etrema-usa.com/documents/terfenol.pdf". Etrema Products, Inc. website.

[19] Janocha, H., 2001. "Application potential of magnetic field driven new actuators". Sensors and Actuators A, **91**.

[20] Owen, G. E., 2003. Electromagnetic Theory. Courier-Dover Publications, Chelmsford, MA.